

PIV ANALYSIS OF SOIL DEFORMATION BENEATH A GROUSER WHEEL

Yosuke Yamano^a, Kenji Nagaoka^a, and Kazuya Yoshida^a

^a*Tohoku University, {yamano,nagaoka,yoshida}@astro.mech.tohoku.ac.jp*

Abstract

This paper presents an analysis of soil deformation beneath a grouser wheel based on particle image velocimetry (PIV). So far, wheeled mechanism has been mainly adopted in locomotion gears of exploration rovers on lunar and planetary surfaces because of its reliability and efficiency. Such surfaces are generally covered with fine soil such as lunar or Martian regolith. Thus, plate-like lugs, called grousers, have been successfully attached to wheels to improve their mobility performance. However, a reasonable model of the grouser wheel traveling on soil has not been established. Accordingly, understanding the soil-wheel interaction including soil deformation beneath the grouser wheel is a key approach for modeling. In this paper, we elaborate an experimental analysis of soil deformation and flow beneath a grouser wheel. We measured the wheel rotational angle, wheel sinkage, traveling distance, and consecutive images captured by a high-resolution digital camera fixed perpendicular to a sandbox through experiments. The time histories of flow velocity of the soil particles are calculated using a particle image velocimetry (PIV) analysis. Based on the experimental results, we discuss the shape of the slip-line and thickness of the soil flow under several conditions of wheel slippage and sinkage.

Keywords: PIV analysis, grouser wheel, soil deformation, exploration robots.

1. Introduction

Recently, various lunar and planetary exploration missions have been planned and operated by major development countries. A robotic mission using mobile robots, the so-called *rovers*, is a possible means for advanced exploration on the Moon and Mars. In particular, wheeled rovers have played a significant role in the past and in the ongoing Mars missions undertaken by NASA. These rover missions have proven that unmanned rovers can contribute significantly to detailed geological investigation, and thereby provide significant scientific findings on the surfaces of extraterrestrial bodies. In future missions, rovers are expected to accomplish more challenging exploration missions.

The lunar and planetary surfaces are covered with fine soil such as lunar regolith. Hence, wheeled rovers can easily slip and become stuck on the soil. To avoid such critical situations, it is necessary to design, develop, and operate a rover system based on wheel-soil interaction. The fundamentals of the mechanical interaction between a running gear and soil have been researched in terms of soil mechanics (Bekker 1956; Wong 2008). Most of the previous studies have focused on relatively-larger wheels that can be modeled as simplified wheels without plate-like lugs or grousers. Although these wheel-soil interaction models have been widely applied to terrain identification (Iagnemma and Dubowsky 2004), motion control (Iagnemma and Dubowsky 2004; Ishigami et al. 2009), or prediction of tractive limitations (Nagaoka et al. 2012), it is well-known that grousers attached to the wheel surface can enhance the mobility performance of wheels and are essential components for traveling on loose soil. We have measured soil reaction force acting on a grouser wheel (Higa et al. 2016), and thereby clarified that the reaction force distributions are drastically

The authors are solely responsible for the content of this technical presentation. The technical presentation does not necessarily reflect the official position of the International Society for Terrain Vehicle Systems (ISTVS), and its printing and distribution does not constitute an endorsement of views which may be expressed. Technical presentations are not subject to the formal peer review process by ISTVS editorial committees; therefore, they are not to be presented as refereed publications. Citation of this work should state that it is from an ISTVS meeting paper. EXAMPLE: Author's Last Name, Initials. 2014. Title of Presentation. The 10th Asia-Pacific Conference of ISTVS, Kyoto, Japan. For information about securing permission to reprint or reproduce a technical presentation, please contact ISTVS at 603-646-4405 (72 Lyme Road, Hanover, NH 03755-1290 USA)

different from stress distributions acting on a *grousers-less* wheel, defined here as a wheel without grousers or with low grousers as slip resistance on the wheel surface. Although our previous research reported the measurement of this interaction force, a reasonable model of a grouser wheel traveling on soil has not been established. In addition to the force measurement, understanding the soil deformation characteristics beneath the grouser wheel is a key approach for modeling. With recent progression of image processing technology and computational processing capability, it has become possible to visualize soil flow from continuous camera images without physical contact by using particle image velocimetry (PIV). PIV-based analysis enables one to obtain the velocity of massive soil particles. PIV has been applied to the analysis of soil deformation beneath a *grouser-less* wheel (Senatore et al. 2013; Skonieczny et al. 2014). However, the PIV analysis for the grouser wheel is currently lacking.

In this paper, we present a PIV analysis of soil deformation and flow beneath a grouser wheel traveling on soil. From the PIV-based observation of soil flow, the soil deformation under interaction with the grouser wheel is quantitatively discussed using single wheel experiments. In particular, to observe soil flow without the interference of multi-grousers, we used a single-grouser wheel for the PIV analysis.

2. Single Wheel Testbed

Fig. 1 shows the experimental apparatus of a single-grouser wheel for the PIV-based analysis, where a multi-grouser is illustrated in Fig. 1(b) for generality. The sandbox has a length, width, and depth of 1.6 m, 0.3 m, and 0.3 m, respectively, and is filled with Toyoura sand. As mentioned before, to accurately understand the characteristics of the soil flow caused by the grouser, a single-grouser wheel was used in this study, as shown in Fig. 1(c). The specifications of this single-grouser wheel are as follows: the wheel diameter is 200 mm, the wheel width is 100 mm, the height of the grouser is 25 mm, the thickness of the grouser is 5 mm, and the total weight acting on the wheel is 1.6 kg. The wheel can achieve free motion in vertical and horizontal directions, and the displacement in each direction was measured using a linear encoder.

The single wheel testbed has a glass-walled observation window to capture the soil flow beneath the wheel using a digital camera. The position of the camera was fixed on the floor with a tripod at the height of 235 mm and distance of 320 mm from the target window, and the frame rate of the camera was set to 60 fps. In addition, to simulate various wheel slip conditions, a traction load was applied to the wheel horizontally (see Fig. 1(b)). Throughout the experiments, the rotational velocity of the wheel was controlled to be constant and its rotational angle was obtained using a rotary encoder.

3. Accuracy Evaluation of PIV

Prior to the single-grouser wheel experiments, the accuracy of PIV analysis was evaluated.

3.1 Measurement Method

An evaluation experiment was carried out to compare the PIV method with ground truth values. In this experiment, the digital camera was moved in the horizontal direction by maintaining a distance of 235 mm from the glass window of the sandbox. A velocity vector of the soil particle was computed based on PIV processing of the camera images. The accuracy of the PIV-based analysis was evaluated by comparing its resulting velocity and the horizontal velocity obtained using the linear encoder, which is a ground truth. Here, as shown in Fig. 2(a), the velocity vectors of soil flow, which is obtained in the field of view, were used for calculating the average velocity.

3.2 Results

Fig. 2 shows the experimental results of the evaluation of PIV accuracy. The processed image confirmed that the horizontal motion was calculated based on the velocity vector as indicated by light-green-colored arrows in Fig. 2(a). From the comparison results shown in Fig. 2(b), the velocity obtained using PIV coincides with the velocity obtained

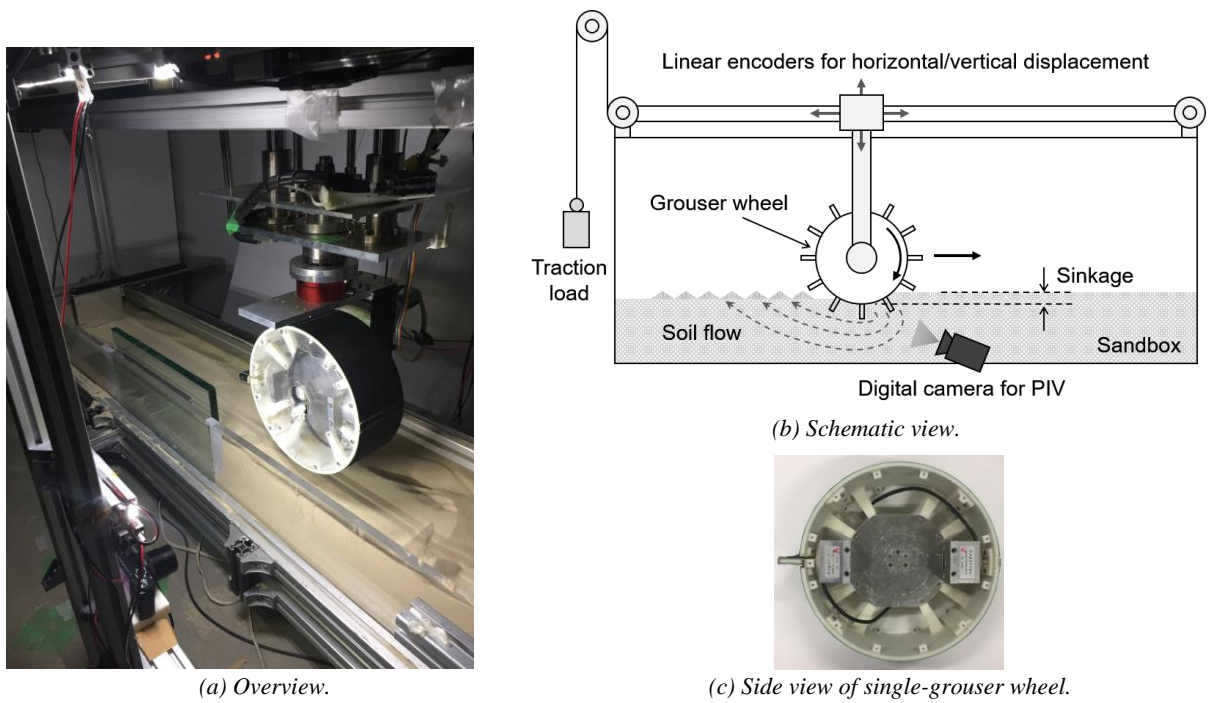


Fig. 1. Experimental apparatus of single-grouser wheel for PIV analysis.

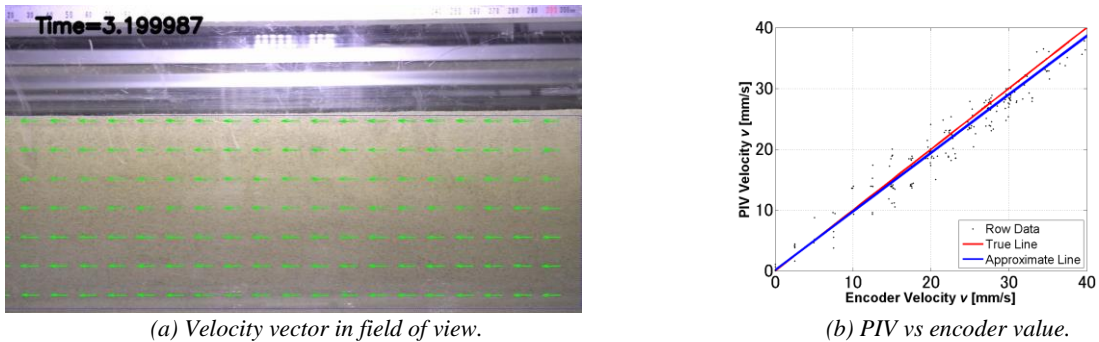


Fig. 2. Experimental results of accuracy evaluation of PIV.

using the linear encoder at various velocity values. Thus, this experiment concludes that the PIV analysis is sufficiently accurate to track the soil flow over a wide velocity range.

4. Soil Flow Analysis

4.1 Experimental Conditions

In the experiments for the analysis of soil flow, the wheel angular velocity was controlled to be 1.6 rad/s. To simulate different wheel slip conditions, several traction loads (10, 15, 20, 25, and 30 N) were applied. As a common initial condition, the single-grouser was set parallel to the soil surface, i.e., the traveling direction of the wheel and the wheel angle of 90° . Furthermore, a wheel angle is defined as a wheel rotational angle. Thus, when the wheel angle is 0° , the single-grouser is located immediately beneath the wheel and the line connecting the wheel axle with the grouser is vertical.

Thus, to evaluate the slip state of the grouser wheel, the slip ratio, S , is defined as follows:

$$S = \frac{(r+l)\omega - v}{(r+l)\omega} \quad (1)$$

where v is the actual velocity in the horizontal direction, ω is the angular velocity of the grouser wheel, r is the radius of the wheel, and l is the height of the grouser. The flow vector of the soil particles is indicated by a red-colored arrow in the images captured by the camera.

4.2 Results and Discussion

4.2.1 Velocity Vector of Soil Particles

Fig. 4 shows the experimental results of visualization of the soil flow at $S = 21.5\%$ and 81.3% , where the results for the wheel angles of 40° , 30° , 20° , and 10° are shown. The results confirm that the soil flow is generated opposite to the direction of the motion of the grouser. Moreover, from the results for the wheel angles of 40° and 30° at $S = 21.5\%$, the soil velocity is low compared with that under the other conditions. The range of the slip-line field (i.e., soil failure region) varies with a change in the wheel angle and slip. This change in the slip-line field depends on the wheel motion.

4.2.2 Shape of Slip Line

Given that the velocity vectors in the x (horizontal) and y (vertical) directions are u and v , respectively, a streamline as a two-dimensional steady flow can be expressed as follows:

$$\frac{dx}{u} = \frac{dy}{v} \quad (2)$$

Based on Eq. (2), we can depict the slip-line so that the velocity vector becomes a tangent line at each curved point, where the initial position of the slip-line is set on the grouser tip.

Fig. 5 shows the results of superimposing the identified slip-line on the PIV-processed images where the wheel angles are 20° and 10° at $S = 52.4\%$. Reasonable slip-lines can be tracked in each condition using the streamline analysis given in Eq. (2). Furthermore, Fig. 6 shows the slip-line shape under various slip ratios, where the initial position of the slip-line is commonly set to $(X, Y) = (0, 0)$. The resulting plots confirm that most slip-line fields (soil failure regions) are generated up to a depth greater than the depth of the grouser tip position. When the wheel angle is small, the soil failure region becomes small, and shear failure is caused in a shallow region. In contrast, when the wheel angle is large, the slip-line shape becomes a relatively large arc.

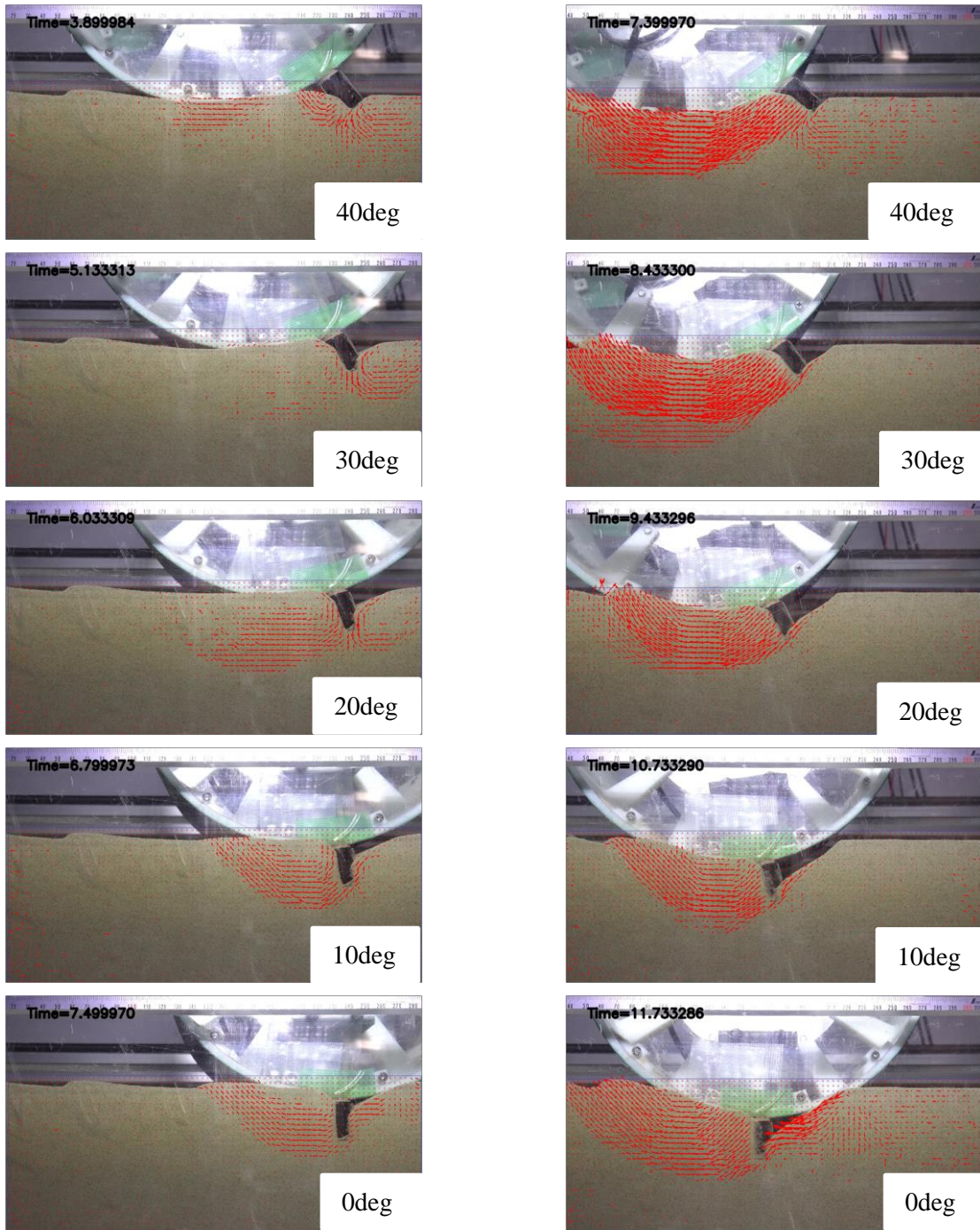
4.2.3 Thickness of Sand Flow Field

The distance from the grouser tip to the deepest point of the slip-line and the angle of the maximum flow thickness are respectively defined as the maximum flow thickness and λ , where λ is the angle formed by the line connecting the wheel axle and the point farthest from the slip line and the y -axis, as shown in Fig. 7.

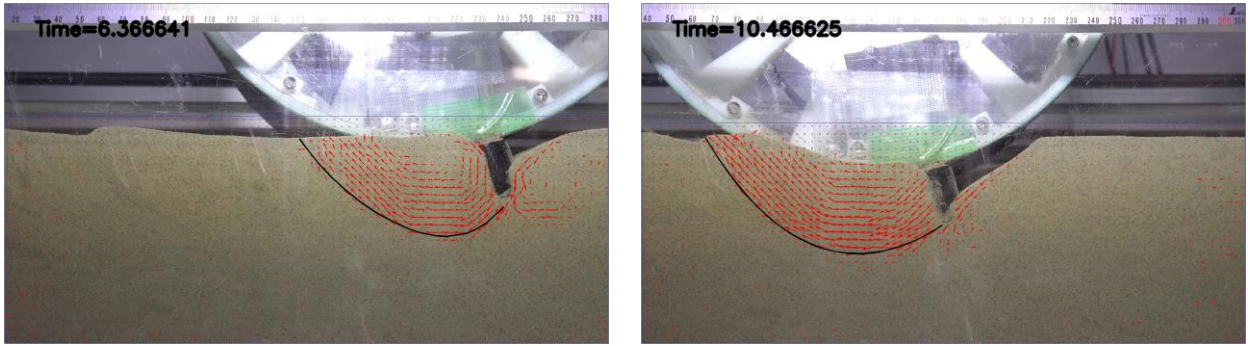
Furthermore, as the sampling rate of the linear encoders is different from that of the digital camera, time synchronization was performed using a linear interpolation as follows:

$$y = \frac{y_{i+1} - y_i}{t_{i+1} - t_i} t + y_i - \frac{y_{i+1} - y_i}{t_{i+1} - t_i} t_i \quad (3)$$

where y_i is the traveling distance or sinkage at time t , and t_i is the increment value of $1/60$ s. From Eq. (3), the angle between the wheel axle and the maximum flow thickness can be calculated.



(a) $S = 21.5\%$ (b) $S = 81.3\%$
Fig. 4. Angle histories of soil flow beneath the single-grouser wheel based on PIV analysis.



(a) Wheel angle of 20°

(b) Wheel angle of 10°

Fig. 5. Resulting slip line at $S = 52.4\%$

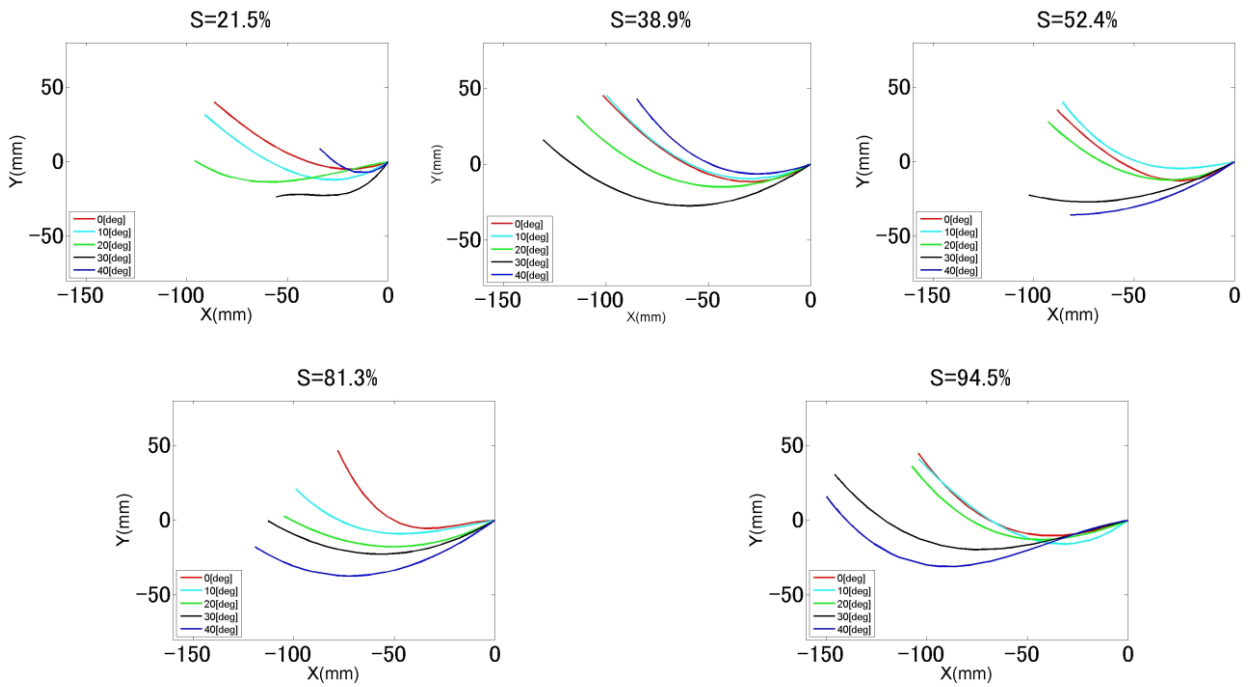


Fig. 6. Resulting slip-lines normalized in XY coordinates.

Fig. 8 shows the thickness of the soil flow field, where the upward direction of the y -axis is positive. From the results, the soil flow thickness increases with an increase in the wheel angle. In particular, when the slip ratio is large, the thickness monotonically increases. Fig. 9 shows the angle λ shown in Fig. 7. The results confirm that the maximum soil flow thickness is observed in the approximately same direction at each slip ratio.

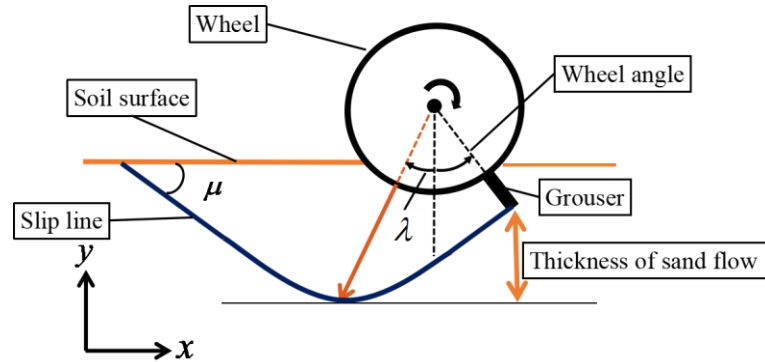


Fig. 7. Diagram illustrating the relationship between the slip line and a grouser wheel

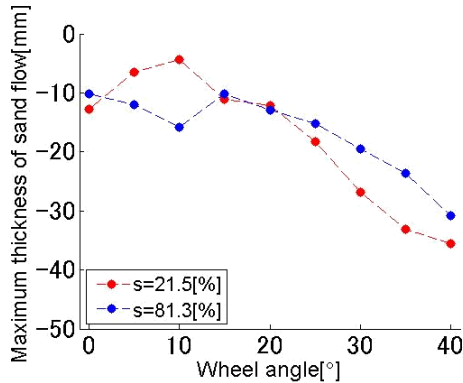


Fig. 8. Thickness of soil flow field.

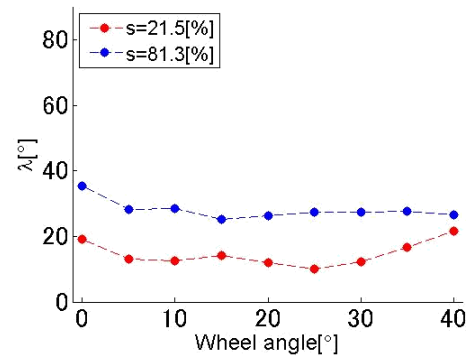


Fig. 9. Angle of thickness of soil flow field.

4.2.4 Soil Failure Angle

The soil failure angle is defined as shown in Fig. 7, where μ represents the angle between the soil surface according to the theory of soil mechanics and is given follows:

$$\mu = \frac{\pi}{4} - \frac{\phi}{2} \quad (4)$$

where ϕ is the internal friction angle of soil. Comparison between the soil failure angles of the experiments and the theory is shown in Fig. 10. Hence, the theoretical value of μ can be calculated as 26° , where the value of μ is given in degrees for ease of understanding. From Fig. 10, however, the soil failure angle is much larger than 26° at each traction load. This difference suggests that soil failure caused by the grouser wheel is not a typical soil failure state, and remodeling of the soil failure is required depending on the wheel motion.

5. Conclusion

In this paper, we presented an analysis of soil deformation beneath a grouser wheel based on PIV and showed the resulting soil flow beneath a single-grouser wheel under various slip conditions. From the results, one of the soil deformation characteristics, i.e., the soil slip-line, is discussed under several slip conditions. In addition to the comparison of the shapes of the slip-line and the flow velocities on it under various slip ratios, the thickness of the soil failure field is discussed. In particular, unlike conventional soil failure theory, the soil failure angle changes depending on the wheel motion. This is a key aspect for modeling the grouser wheel. Based on the results of this study, we will address the PIV-based analysis and modeling of the wheel with multi-grousers in the future.

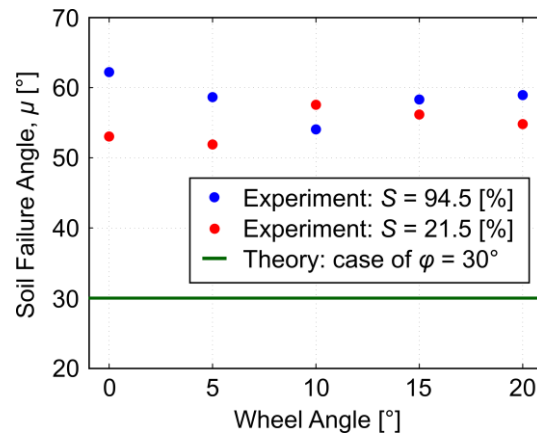


Fig. 10. Comparison of soil failure angle.

Acknowledgments

This work was supported by JKA and its promotion funds from KEIRIN RACE.

References

- Bekker, M.G., 1956. Theory of Land Locomotion. University of Michigan Press, Ann Arbor, MI.
- Iagnemma, K., Dubowsky, S., 2004. Mobile robots in rough terrain. Springer, New York, NY.
- Ishigami, G., Nagatani, K., Yoshida, K., 2009. Slope traversal controls for planetary exploration rover on sandy terrain. J. Field Robot. 26(3), 264–286.
- Nagaoka, K., Mizukami, N., Kubota, T., 2012. Prediction of tractive limitations of a rigid wheel on loose soil. J. Asian Electric Veh. 10(1), 1583–1590.
- Higa, S., Sawada, K., Nagaoka, K., Nagatani, K., Yoshida, K., 2016. Measurement of stress distributions of a wheel with grousers traveling on loose soil. In: 2016 IEEE Int. Conf. on Robot. Automat., pp. 2828–2833.
- Senatore, C., Wulfmeier, M., Vlahinic, I., Andrade J., Iagnemma, K., 2013. Design and implementation of a particle image velocimetry method for analysis of running gear-soil interaction. J. Terramech. 50(5-6), 311–326.
- Skonieczny, K., Moreland, S.J., Asnani, V.M., Creager, C.M., Inotsume, H., Wettergreen, D.S., 2014. Visualizing and analyzing machine-soil interactions using computer vision. J. Field Robot. 31(5), 820–836.
- Wong, J.Y., 2008. Theory of Ground Vehicles (fourth edition). John Wiley and Sons, Inc., Hoboken, NJ.